JOURNAL OF AIRCRAFT
Vol. 46, No. 3, May–June 2009

Application of a Pendulum Support Test Rig for Aircraft Stability Derivative Estimation

A. Gatto*
Brunel University, Uxbridge, England UB8 3PH, United Kingdom

DOI: 10.2514/1.38916

This paper presents a novel technique for extracting longitudinal stability derivative information from an actively controlled wind-tunnel test model. The technique, designated as the pendulum support rig, uses a test model mounted inverted and suspended from the wind-tunnel roof via a supporting strut and a single-degree-of-freedom gimbal providing model motion in heave and forward translation. An additional single-degree-of-freedom gimbal connecting the model to the support strut was also used to allow model rotation in pitch. Overall, the technique was found to perform well at predicting the dominant longitudinal stability and control derivatives. This was assessed primarily against the results from an existing established technique obtained by an independent source and from results obtained by the author in a previous investigation, using a different technique.

Nomenclature

C_D	=	drag force coefficient
C_L	=	lift force coefficient
C_m	=	pitching moment coefficient
$\bar{c}$	=	mean aerodynamic chord, m
cb	=	pendulum counterbalance
g	=	acceleration due to gravity, $\mathrm{m} \cdot \mathrm{s}^{-2}$
I_{yy}	=	moment of inertia in pitch, $\mathrm{kg} \cdot \mathrm{m}^2$
M	=	mass, kg
m	=	aerodynamic pitching moment, $\mathrm{N} \cdot \mathrm{m}$
mod	=	wind-tunnel model
q	=	pitch rate, $\mathrm{rad} \cdot \mathrm{s}^{-1}$
R	=	pendulum strut force, N
r	=	pendulum support rig strut length, m
S	=	model reference area, m^2
st	=	pendulum strut
$\mathrm{st}_{\mathrm{c.g.}}$	=	pendulum strut center of gravity
$\mathrm{st}_{\mathrm{c.p.}}$	=	pendulum strut center of pressure
t	=	time, s
V_o	=	freestream velocity, $\mathrm{m} \cdot \mathrm{s}^{-1}$
X, Z	=	global axis coordinate system
x, z	=	coordinates from roof pivot to counterbalance mass, m
α	=	angle of attack, rad
γ	=	pendulum support rig heave angle, rad
ε	=	gimbal pitch angle, rad
η	=	stabilator angle, rad, deg
θ	=	pitch angle, rad
ϕ	=	fixed counterbalance angle, rad

I. Introduction

THE search for new and improved experimental wind-tunnel test techniques to characterize static and dynamic aircraft stability metrics is an ongoing and often difficult endeavor. One of the primary reasons for the inability of current methods to ascertain a global assessment of static and dynamic stability information is the need for extremely versatile, cost-effective, and robust test rigs that can accurately measure the performance of the model under differing setup configurations. Additionally, these techniques require the minimization of uncertainty from tare interference while simultaneously measuring motion and load data. Many of the currently used test rigs can perform some of the these tasks relatively well. However, these systems typically involve excessive initial setup expenditures, large operating costs, and bulky apparatus [1,2]; have limited motion capabilities [3–8]; possess significant intrusive and interference effects [9,10]; and/or have undue mechanical complexities requiring advanced control and management architectures [3,4,11–18]. In lieu of these widely accepted inadequacies, a proposed new tool for the extraction of stability derivative information from an arbitrary subscale test model is presented in this paper.

Broadly defined as the pendulum support rig (PSR) and shown in Fig. 1, this technique uses an actively controlled model that is suspended inverted from the roof of a wind tunnel. Two gimbals, one connecting a support strut to the tunnel roof and another connecting the strut to the model, give the setup free motion in model pitch and constrained motion in model heave and forward translation. Measurements of angular position taken from these two instrumented gimbals, together with the use of an intrinsic measurement of the model control surface deflection, allow, through parameter estimation and optimization techniques, evaluation of stability derivative information.

The concept of the PSR was first introduced by Goman et al. [19], with a primarily theoretical subsequent investigation published later by the same author in [20]. In the later reference, the theoretical background to the concept, detailing both the 2-DOF (degree of freedom) and a more elaborate 5-DOF system was presented, which included model roll, yaw, and sway. In both instances, the equations of motion were modeled using a generic test model suspended upright in a wind tunnel by an idealized, massless, infinitely stiff, support strut extending up from the wind-tunnel floor. Curious among the results reported from the analysis was the discovery of conditions for some of the model trim angles investigated of an inherent instability in the system, ultimately leading to the development of large-amplitude pendulum strut motions. This inherent stability anomaly was described to result from model *emersion* [20] at increased pendulum strut angles with subsequent contributing/amplifying factors, under actual test conditions, suggested to result from variations in upstream flow conditions, extraneous mechanical vibrations, asymmetric nonlinear aerodynamic/structural coupling, and/or tunnel wall effects. The effect of the strut length was also considered in this publication, with longer strut lengths found to initiate small-amplitude oscillations of aircraft angle of attack. Incursions of the model to higher ranges of angle of attack were also found to create large, often unstable, heave amplitudes; however, it is noted by Goman [20] that the generation of these large-amplitude motions need not preclude the use of the technique as a possible tool

Received 9 June 2008; revision received 14 February 2009; accepted for publication 25 February 2009.

*Lecturer in Aerospace Engineering, Department of Mechanical Engineering, School of Engineering Design. Member AIAA.

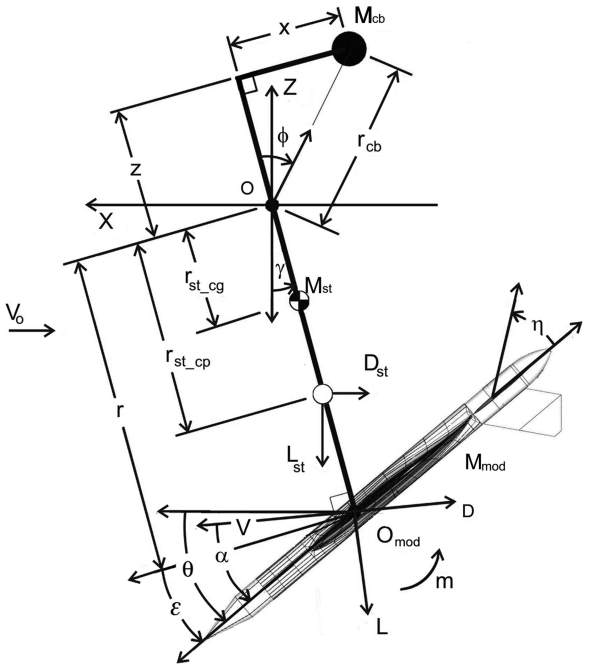

Fig. 1 Schematic of the 2-DOF setup.

for the extraction of stability derivatives, only that for this to occur, the oscillation should be stable and controllable to a sufficient degree, and for a sufficient period, to allow the accurate extraction of model and rig motion data.

Work followed on from Goman [20] with several experimentally based publications on the PSR concept [21–23]; however, much of this work centered on the modeling of limit-cycle behavior and not parameter estimation. Kyle [22] briefly investigated the ability of the PSR to extract stability derivative data with some success; however, some questions over the accuracy of the data, particularly control surface position and upstream flow conditions, were evident in the results presented. Unfortunately, like experimental results presented by Goman et al. [19] and Goman [20], Kyle [22] also documented several problems with the stability and control aspects of the 2-DOF PSR, in particular, the existence of large-scale unstable oscillations, causing the model to traverse outside the region of interest of the open-jet wind-tunnel test section used. This undesirable characteristic of the PSR was argued to be caused by airflow interactions with the support system and the coupled nonlinear rig setup aerodynamics. Kyle [22] also made attempts to separate the pitch rate and acceleration derivatives, but unfortunately, due primarily to the lack of quality data obtained, achieved little success.

In this paper, the ability of the PSR to be used as a viable tool for the extraction of stability derivative data from an actively controlled generic test model is shown. The investigation centers primarily on the 2-DOF PSR configuration and the ability of this setup to accurately estimate longitudinal stability derivative information for the model. Ultimately, this ability is evaluated from comparisons between the results obtained from the 2-DOF configuration against another established test method and one used by the author in an earlier investigation.

II. Two-Degree-of-Freedom Equations of Motion

Figure 1 gives a schematic representation of the inverted 2-DOF PSR configuration considered in this investigation. As shown in the figure, position O locates the roof gimbal pivot position of the pendulum strut relative to the wind-tunnel roof with the model gimbal pivot position for the model center of gravity at the other end of the support strut, located at O_{mod}. From the configuration shown, the position and orientation of the model at any instant can be described by the heave angle γ, length of the exposed pendulum strut r, counterbalance mass M_{cb}, and radius r_{cb}, together with the gimbal pitch angle ε at O_{mod}. In reality, however, factors such as nonzero support structure mass and associated aerodynamic influences (modeled as shown in Fig. 1), together with model c.g. (center of gravity) and a.c. (aerodynamic center) spatial offsets from the model gimbal pivot position, all impart influences of varying degrees on the resulting motion. However, for simplicity in the derivation of the equations of motion, the aerodynamic forces and moments on the model, as well as its center of gravity, were assumed to act through the gimbal pivot position at O_{mod}. A counterbalance mass that is used to both set the trim static heave angle of the complete system and dictate the range of heave angle achieved is shown atop the support strut, located 90 deg aft of the support-strut axis.

Therefore, from analysis of the geometry of Fig. 1, we obtain expressions for the position of the model, counterbalance mass, and c.g. of the support strut as

$$X_{\text{mod}} = -r\sin\gamma \qquad Z_{\text{mod}} = -r\cos\gamma \qquad X_{\text{st}_{\text{c.g.}}} = -r_{\text{st}_{\text{c.g.}}}\sin\gamma$$
$$Z_{\text{st}_{\text{c.g.}}} = -r_{\text{st}_{\text{c.g.}}}\cos\gamma \qquad X_{\text{cb}} = -r_{\text{cb}}\sin(\phi-\gamma) \qquad (1)$$
$$Z_{\text{cb}} = r_{\text{cb}}\cos(\phi-\gamma)$$

where $r_{\text{cb}} = \sqrt{x^2+z^2}$. Differentiating with regard to time and because $\dot{r}=0$, $\dot{r}_{\text{cb}}=0$, and $\dot{r}_{\text{st}_{\text{c.g.}}}=0$, we obtain

$$\dot{X}_{\text{mod}} = -r\cos(\gamma)\dot{\gamma} \qquad \dot{Z}_{\text{mod}} = r\sin(\gamma)\dot{\gamma}$$
$$\dot{X}_{\text{st}_{\text{c.g.}}} = -r_{\text{st}_{\text{c.g.}}}\cos(\gamma)\dot{\gamma} \qquad \dot{Z}_{\text{st}_{\text{c.g.}}} = r_{\text{st}_{\text{c.g.}}}\sin(\gamma)\dot{\gamma} \qquad (2)$$
$$\dot{X}_{\text{cb}} = r_{\text{cb}}\cos(\phi-\gamma)\dot{\gamma} \qquad \dot{Z}_{\text{cb}} = r_{\text{cb}}\sin(\phi-\gamma)\dot{\gamma}$$

Using Eq. (2), the total kinetic energy of the system is represented as

$$\text{KE} = \frac{M_{\text{mod}}(\dot{X}_{\text{mod}}^2+\dot{Z}_{\text{mod}}^2)}{2} + \frac{M_{\text{cb}}(\dot{X}_{\text{cb}}^2+\dot{Z}_{\text{cb}}^2)}{2} + \frac{M_{\text{st}}(\dot{X}_{\text{st}_{\text{c.g.}}}^2+\dot{Z}_{\text{st}_{\text{c.g.}}}^2)}{2} + \frac{I_{yy}\dot{\theta}^2}{2} \qquad (3)$$

Which gives, when substituting Eq. (2) in Eq. (3),

$$\text{KE} = \frac{M_{\text{mod}}r^2\dot{\gamma}^2}{2} + \frac{M_{\text{cb}}r_{\text{cb}}^2\dot{\gamma}^2}{2} + \frac{M_{\text{st}}r_{\text{st}_{\text{c.g.}}}^2\dot{\gamma}^2}{2} + \frac{I_{yy}\dot{\theta}^2}{2} \qquad (4)$$

Also from Fig. 1, the potential energy of the system is given by

$$\text{PE} = g(M_{\text{mod}}Z_{\text{mod}} + M_{\text{cb}}Z_{\text{cb}} + M_{\text{st}}Z_{\text{st}_{\text{c.g.}}}) = -M_{\text{mod}}gr\cos\gamma + M_{\text{cb}}gr_{\text{cb}}\cos(\phi-\gamma) - M_{\text{st}}gr_{\text{st}_{\text{c.g.}}}\cos\gamma \qquad (5)$$

Using the following Lagrange equations with $L = \text{KE} - \text{PE}$ to determine the equations of motion,

$$\frac{d}{dt}\left(\frac{\partial L}{\partial\dot{\gamma}}\right) - \frac{\partial L}{\partial\gamma} = Q_\gamma \quad \text{and} \quad \left(\frac{d}{dt}\left(\frac{\partial L}{\partial\dot{\theta}}\right) - \frac{\partial L}{\partial\theta}\right) = Q_\theta \qquad (6)$$

where

$$L = \frac{M_{\text{mod}}r^2\dot{\gamma}^2}{2} + \frac{M_{\text{cb}}r_{\text{cb}}^2\dot{\gamma}^2}{2} + \frac{M_{\text{st}}r_{\text{st}_{\text{c.g.}}}^2\dot{\gamma}^2}{2} + \frac{I_{yy}\dot{\theta}^2}{2} + M_{\text{mod}}g(r\cos\gamma) - M_{\text{cb}}gr_{\text{cb}}\cos(\phi-\gamma) + M_{\text{st}}r_{\text{st}_{\text{c.g.}}}g\cos\gamma \qquad (7)$$

We obtain the following equations of motion for the 2-DOF system:

$$(M_{\text{mod}}r^2 + M_{\text{cb}}r_{cb}^2 + M_{\text{st}}r_{\text{st}_{\text{c.g.}}}^2)\ddot{\gamma} + M_{\text{mod}}gr\sin\gamma + M_{\text{cb}}gr_{\text{cb}}\sin(\phi-\gamma) + M_{\text{st}}r_{\text{st}_{\text{c.g.}}}g\sin\gamma = r\frac{\rho V^2 S}{2}[C_L\sin\gamma - C_D\cos\gamma] + r_{\text{st}_{\text{c.p.}}}\frac{\rho V^2 S_{\text{st}}}{2}[C_{L_{\text{st}}}\sin\gamma - C_{D_{\text{st}}}\cos\gamma] \qquad (8)$$

where $V = \sqrt{(V_o + \dot{X}_{\text{mod}})^2 + \dot{Z}^2_{\text{mod}}}$ and

$$\ddot{\theta} I_{yy} = m_\theta \tag{9}$$

If we neglect gimbal friction, the following relationships exist for Q_γ, Q_θ, R_γ, m_{st}, m, C_L, C_m, and C_D:

$$Q_\gamma = rR_\gamma + m_{\text{st}}, \qquad Q_\theta = m_\theta \tag{10}$$

$$R_\gamma = \frac{\rho V^2 S}{2}[C_L \sin\gamma - C_D \cos\gamma] \tag{11}$$

$$m_{\text{st}} = r_{\text{st}_{\text{c.p.}}} \frac{\rho V^2 S_{\text{st}}}{2}[C_{L_{\text{st}}} \sin\gamma - C_{D_{\text{st}}} \cos\gamma] \tag{12}$$

$$m = \frac{\rho V^2 S \bar{\bar{c}}}{2} C_m \tag{13}$$

$$\begin{aligned} C_{L,m} &= C_{Lo,mo} + C_{LV,mV}\frac{\Delta V}{V} + C_{L\alpha,m\alpha}\Delta\alpha \\ &+ C_{L(q+\dot{\alpha}),m(q+\dot{\alpha})}\frac{(q+\dot{\alpha})\bar{\bar{c}}}{2V} + C_{L\eta,m\eta}\Delta\eta \\ &\text{and} \quad C_D = C_{Do} + kC_L^2 \end{aligned} \tag{14}$$

III. Experimental Setup and Procedure

A. M2370 Flight Vehicle

A general layout of the QinetiQ, Ltd., designated full-scale M2370 vehicle used for all testing is shown in Fig. 2. The model was of carbon-fiber construction with a diamond-wing planform and leading-edge strakes running along the majority of the leading portion of the central fuselage. Facilitated in the design of the model was a 30 mm adjustment in the distance between the c.g. and the a.c. of the model. This was achieved through the movement of a cavity tray mounted inside the fuselage. A list of general aerodynamic dimensions and characteristics are outlined in Fig. 2, as provided by QinetiQ, Ltd.

B. Instrumentation and Hardware

The M2370 flight vehicle supplied by QinetiQ, Ltd., used all moving stabilators, rudder, and ailerons. All of these control surfaces were driven by digital servos and controlled through a dedicated driver board with an RS232 interface. This port was attached to a DIMM-PC running control software written by QinetiQ, Ltd. Measurement of each control surface position was obtained through coupled precision potentiometers, resulting in a control surface calibration accuracy under no-load conditions of less than ± 2.5 deg. All data from the control surfaces were sampled at 50 Hz using a Diamond MM-33-AP data acquisition board and automatically stored to a flash memory card located in the tail assembly for later analysis.

The wind tunnel used for all tests was a 9×7 ft closed-test-section closed-circuit wind tunnel owned by British Maritime Technology

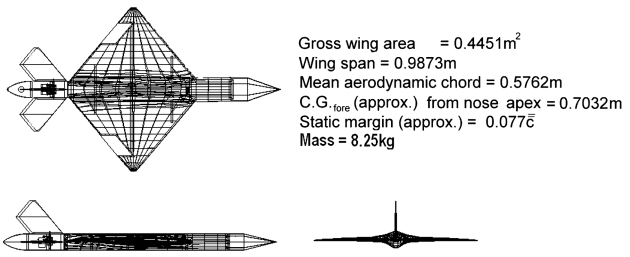

Fig. 2 The M2370 flight vehicle.

located in Teddington, London. The maximum achievable free-stream velocity in the test section is 60 m/s, with the test speed selected for this investigation set to approximately $V_o = 26$ m/s. The control of the tunnel speed was better than 1 m/s, with turbulence intensity rated at 0.25%. Additionally, no blockage corrections or interference effects were considered in this paper.

Control of the M2370 flight vehicle and all data acquisition operations were managed in real time by a dSpace data acquisition system. All data acquired from the PSR setup were sampled via 16-bit precision at 1000 Hz. Data acquisition periods ranged from 20–30 s, depending on the test configuration. The flight vehicle was controlled though an RS232 asynchronous port situated on the controller board of the dSpace hardware, which was connected to the servos' driver board. To excite the model during the dynamic tests, a square impulse of variable amplitudes between ± 5 and ± 10 deg (at 0.2 s duration) was used as the primary initiation mechanism with the model, before excitation, trimmed to a steady and stable flying condition ($\eta \approx -1.6$ deg, $\alpha \approx -1.6$ deg).

For the determination of longitudinal dynamic stability derivatives, the moment of inertia of the M2370 flight vehicle about its pitch axes was determined using the trifilar suspension technique [24] and measured at $I_{yy} = 1.653 \pm 0.053$ kgm^2.

C. Two-Degree-of-Freedom PSR Setup

The PSR operating in 2-DOF used two instrumented gimbals: one mounted inside the model (pitch DOF) and the other mounted to the wind-tunnel roof (heave DOF). Connecting these two gimbals was a purpose-built pendulum support strut (diameter = 0.0381 mm, length = 1.65 m, $r = 1.26$ m, $r_{\text{st}_{\text{c.g.}}} = 0.31$ m, and mass = 5.18 kg) that extended up through the wind-tunnel roof and out of the test section. In this configuration, the model was mounted to the pitch gimbal in an inverted configuration.

The pitch angle of the model was calibrated using a digital inclinometer (error = ± 0.1 deg) placed on the model fuselage and compared against the model gimbal pitch potentiometer (Penny and Giles model D150098) via the dSpace user interface. The uncertainty in angular position after calibration was estimated to be no more than ± 0.5 deg. This degree of accuracy was typical of this setup, with the calibration of the additional measurement potentiometer, located inside the roof gimbal measuring heave angle, also found to reside within this error band.

For the model pitch and heave degrees of freedom, the achievable limits of gimbal angular rotation was approximately ± 45 deg. To reduce impact loads on the two gimbals if these limits were reached, semirigid padding was placed around a cutout in the fuselage of the model as well as limit wires used to connect the top of the pendulum strut to the test-section roof. Because of the extent of angular motion evident for the pitch degree of freedom, the cutout required in the model fuselage was quite large and at high angles of attack would conceivably have introduced extraneous aerodynamic effects on the results. No attempt has been made to account for these effects in the results presented.

Figure 3 shows the model installed inside the wind tunnel in the 2-DOF configuration. To allow access through to the top of the wind tunnel, a circular cutout in the roof was made in which the roof gimbal was installed (Fig. 4). The roof gimbal was purposely designed and built for this task and consisted of three interconnected supporting frames, with the two innermost frames fixed through the use of an installed sway plate. Installation of the plate limited movement of the roof gimbal to heave motion only.

To allow adjustment of the wind-on static heave angle as well as its dynamic range, a counterbalance weight was connected to the end of the pendulum strut protruding from the top of the wind tunnel. This was connected to the strut by a lightweight support structure fixed 90 deg aft to the support-strut axis, which also allowed adjustment of the linear position of the counterbalance weight along its length (x in Fig. 1). After initial investigations into the best magnitude and position of the counterbalance weight, a 40 N weight placed 5.5 cm aft of the pendulum strut axis was chosen as the test condition. Under these conditions, the static heave angle was found to be stable and

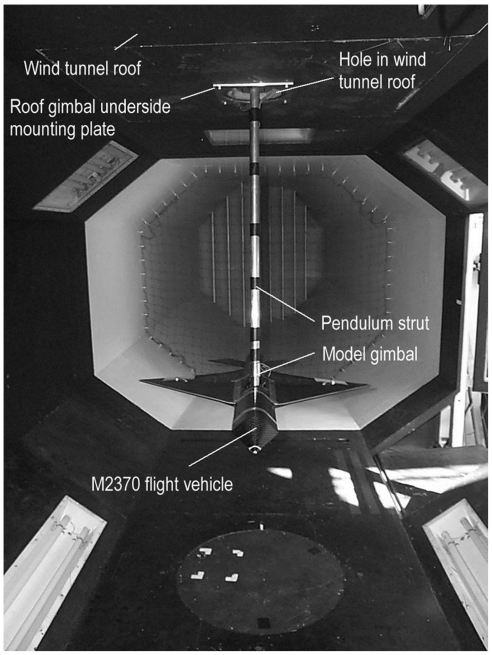

Fig. 3 Model installed in 2-DOF configuration.

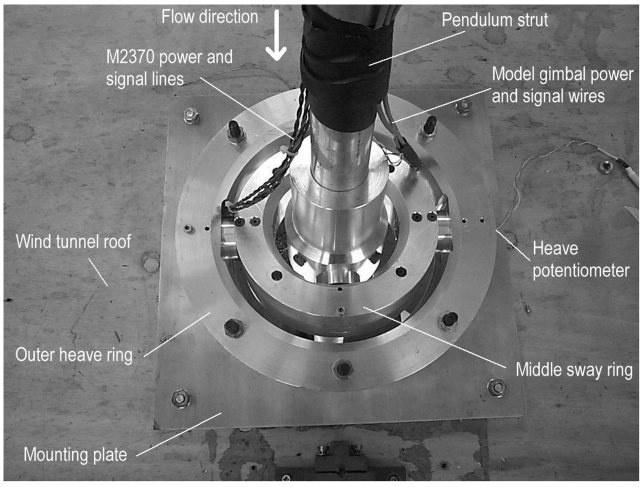

Fig. 4 PSR 2-DOF wind-tunnel roof gimbal.

equalized to a small positive value ($\gamma \approx 0.5$ deg). Additionally, to achieve satisfactory stable flying qualities for the model, both the vertical and longitudinal c.g. positions of the model had to be adjusted. For the vertical c.g. position, several configurations were initially tested. These included the pivot position coincident with the model c.g. and the pivot position located either above or below the model c.g. Only locating the model c.g. below the pivot position (measured relative to the inverted model) gave satisfactory performance. A similar procedure was used by Gatto and Lowenberg [24], with a c.g. offset of 5 mm chosen as the final result. To position the longitudinal c.g. location, ballast was added to either the fore or aft extremities of the model until static balance over the pivot position was achieved. Additional gravitational and/or inertial effects on the resultant model motion from the offset c.g. were not considered further.

Before the initiation of the model test program, an evaluation of the aerodynamic influences of the PSR support strut was conducted under test conditions. These influences are included in Eq. (8). To determine these effects, a dummy PSR support strut of identical length and diameter to the actual PSR support strut was mounted on a Kistler six-component piezoelectric balance, located under the floor of the test section of the wind tunnel. The dummy strut was manufactured to have a rounded end to minimize undue effects from the tip aerodynamics. Once mounted on the balance, a manual adjustment facility designed into the rig allowed adjustment of the relative heave angle of the strut relative to the freestream velocity vector (Fig. 5). From a prior check of the calibration [24] of the Kistler balance, maximum deviations in the results obtained were found to be $\pm 2.5\%$ for lift and drag and $\pm 5\%$ for the pitching moment. A more detailed description of the balance can be found in [25].

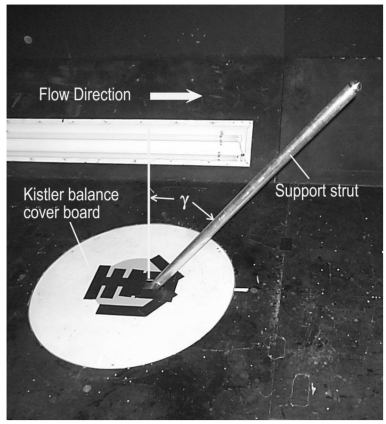

Fig. 5 Experimental setup for PSR support strut tare evaluation.

Results taken to assess the influence of the support strut included static heave angles ranging from −40 to 40 deg in increments of 10 deg. After data collection, lift and drag results were expressed as a function of heave angle through curve-fitting third-order (lift) and second-order (drag) polynomials to the data obtained.

D. Stability Derivative Estimation Procedure

For the estimation of all stability derivatives, nonlinear least-squares MATLAB parameter estimation tools were used. All stability derivatives calculated were modeled with freely adjustable assignments within a large-scale optimization [26] environment. The cost function, which was modeled as the difference between the predicted and experimentally measured results, was minimized through a two-tier optimization procedure. The first stage of the optimization was to find values of the modeled stability derivatives that produced a minimized cost function at a fixed value of aerodynamic transport delay between stabilator initiation and resultant model motion. The second tier of the optimization was to find the optimal transport delay that gave a minimized cost function over the range of transport delays used (0.01–0.4 s). The values of the stability derivatives that gave an ultimate minimized cost function were then used as the final values.

Unless otherwise stated, the optimization process was conducted over a time period of 20 s, with the algorithm used being a subspace trust-region method based on the interior-reflective Newton method [27,28]. All estimated coefficients were assumed to be invariant over the time period specified. Additionally, the optimization algorithm was bounded to exit when the cost-function iterative change fell below a specified tolerance (1×10^{-6}) or exceeded a predefined number of function evaluations (1000). These values were chosen as a tradeoff between overall computation time and an evaluation of the change in final stability derivate estimates at higher tolerance levels.

IV. Results and Discussion

A. Strut Tare Evaluation

Results reduced from analysis of the support-strut aerodynamic influence as a function of heave angle are shown in Fig. 6. As expected, at zero heave angle, the lift is near zero and drag is at a maximum. With heave-angle increase, strut lift oscillates between negative and positive values for positive (aft movement) and negative (fore movement) heave angles. Additionally, the drag produced by the strut undergoes subsequent reductions at both $\gamma < 0$ deg and $\gamma > 0$ deg as the strut becomes more swept relative to

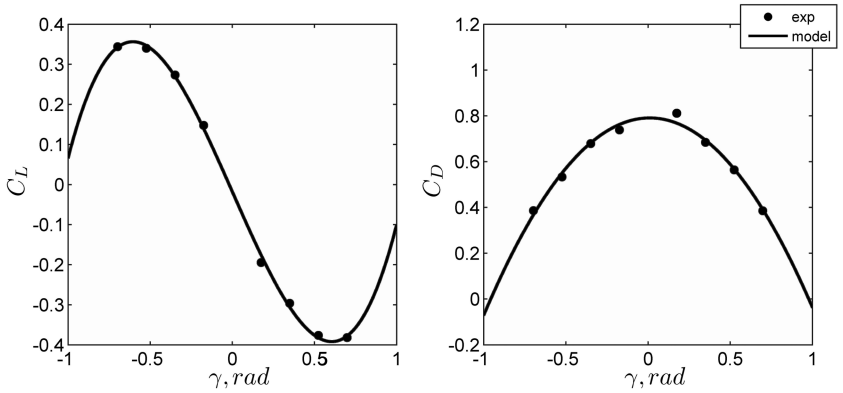

Fig. 6 Strut lift and drag aerodynamics as a function of heave angle.

the freestream velocity vector in both directions. From Fig. 6, the cubic polynomial for the lift and the quadratic polynomial for the drag were constructed for Eq. (8) using coefficients shown in Table 1.

B. Evaluation of Longitudinal Stability Characteristics

1. *Lift-Dependent Stability and Control Derivatives*

Figure 7 shows the results obtained from the parameter estimation routine for the lift-dependent longitudinal control and stability derivatives. Included also in this figure are results for comparison of the same derivatives from a previous test program conducted by QinetiQ, Ltd., using an inexorable drive rig [29–31] and results using a 3-DOF test rig [24] by the author. For all three investigations, the model scale and Reynolds number were identical.

On first inspection, the ability of the 2-DOF PSR and optimization routine to predict viable derivative estimates is very encouraging, with all results presented, excluding the change in lift coefficient due to velocity, indicating good agreement with the reference data included. The increased fidelity of these remaining derivatives was expected, as these derivatives dominate the overall model motion. Results for the lift damping and control derivative, however, do indicate a notable degree of scatter around the reference data, but as shown, possess improved fidelity over results obtained by the author using a 3-DOF test rig [24]. One possible reason for this discrepancy may lie in the differing support structure interference [24] between the two methods used by the author, as opposed to the inexorable drive rig used in the QinetiQ, Ltd., data presented. As noted in [24], results did suggest, particularly for the pitching moment, some influence on stabilator effectiveness when increasingly immersed in the ventral sting wake. Increased correlation between the 2-DOF data and the QinetiQ, Ltd., data seem to suggest that the effect of support interference using the 2-DOF PSR may be less pronounced than that found from using the 3-DOF rig [24].

Generally, results presented for change in lift coefficient due to velocity were found to center around $C_{Lv} \approx 0$, with results for excitation amplitudes between -5 and -10 deg being approximately zero and results between 5 and 10 deg showing increased incoherent scatter. From further analysis of the degree of change in velocity experienced in the 2-DOF tests, it was found that for the maximum stabilator deflection of $\Delta\eta = \pm 10$ deg, the maximum change from the steady-state test speed of 26 m/s was approximately ± 1.3 m/s ($\pm 5\%$ change). It was thought primarily that it was a result of this substantial magnitude mismatch, together with the inherent insensitivity of C_{Lv} to small ranges of velocity change [32,33], which resulted in both the magnitude and uncertainty in the value of C_{Lv} calculated by the optimization routine.

Table 1 Polynomial coefficients for strut aerodynamics model fit

Value	C_L	C_D
A0 γ^3	0.844	——
A1 γ^2	0.001	−0.845
A2 γ	−0.927	0.017
A3	−0.018	0.791
Residual[2]	0.025	0.057

2. *Pitching-Moment-Dependent Stability and Control Derivatives*

From the results presented for the pitching moment derivatives in Fig. 8, the pitching moment control derivative, pitching moment damping derivative, and pitching moment stiffness all show good agreement with the available reference data included. In a similar trend to that observed for the results of the lift-dependent stability and control derivatives shown in Fig. 7, the results for pitching moment derivative due to change in velocity show very little variation from $C_{mv} \approx 0$. Conversely, results for the remaining stability derivatives, with the possible exception of $C_{m\eta}$, do indicate some small variation with change in impulse magnitude, with the tendency to increase in magnitude as the impulse magnitude decreased.

3. *Sample Results of Parameter Estimation Routine Performance*

An example of the typical parameter estimation routine performance to estimate the time-dependent model-lift drag and pitching moment is shown in Figs. 9–11. From Fig. 9, time histories of C_D and C_L indicate trim magnitudes at $t \approx 0$ s of $C_D = 0.077$ and $C_L = -0.087$, respectively (trim conditions $\alpha = -1.6$ deg and $\eta = -1.8$ deg). These values generally agree with results obtained from Gatto and Lowenberg [24] ($C_D = 0.066$ and $C_L = 0.11$ at trim conditions $\alpha = 2.1$ deg and $\eta = -2$ deg); albeit for that investigation, the model was trimmed in a similar flying condition mounted upright. From analysis of the results presented for stabilator performance [24], the control surface was inhibited from achieving the total desired deflection of $\Delta\eta = 10$ deg (actual $\Delta\eta = 9$ deg allowing for trim offset of -1.6 deg), due to inadequacies of the driving mechanism to overcome the aerodynamic loading. Stabilator deflection was also found to produce substantial overshoot when

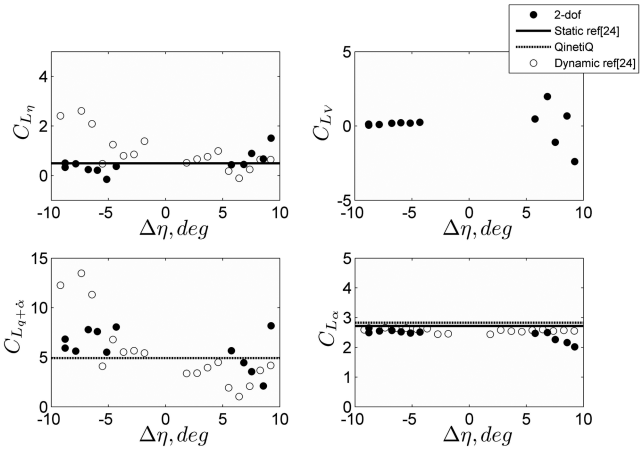

Fig. 7 Results obtained for lift-dependent stability and control derivatives.

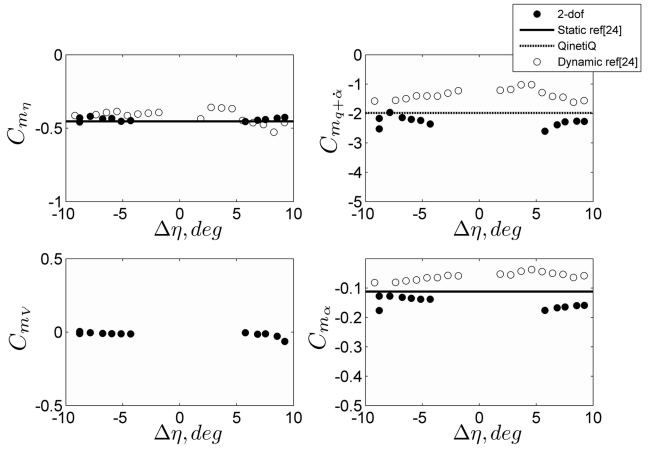

Fig. 8 Results obtained for pitching-moment-dependent stability and control derivatives.

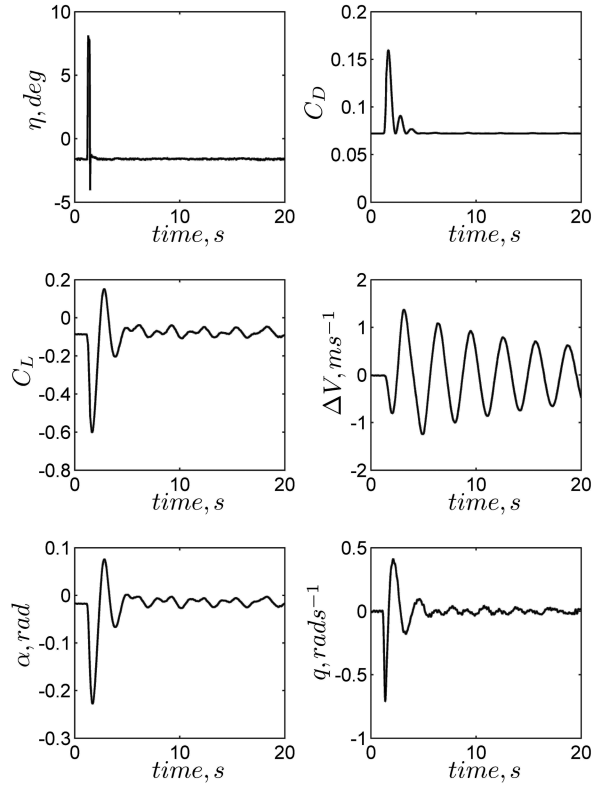

Fig. 9 Example of time histories from parameter estimation optimization routine for lift and drag; $\Delta\eta = 10$ deg.

settling back to $\Delta\eta = 0$ deg. This is shown in Fig. 9 and was measured at $\Delta\eta = 2.5$ deg.

For the 2-DOF testing method, the model trim angle of attack for the flying condition selected was approximately -1.6 deg. From this condition, and with positive stabilator deflection, the model angle of attack is shown to rapidly move through $\alpha \approx -0.22$ rad (-12.6 deg) before reversing direction and passing through $\alpha = 0$ at $t \approx 3$ s. At this position of maximum angle of attack, both C_L and C_D reach values of -0.6 and 0.16, respectively. The subsequent time histories thereafter decay under damped vibration back to a steady-state condition. From the peak in $C_D = 0.16$ at $t \approx 3$ s, two subsequent peaks of diminishing magnitude are also shown and represent increases in drag experienced from corresponding increases in C_L.

Figure 10 shows a comparison of the tangential strut force R_γ predicted using the experimental motion data obtained from the 2-DOF gimbals and modeled data using the developed optimization

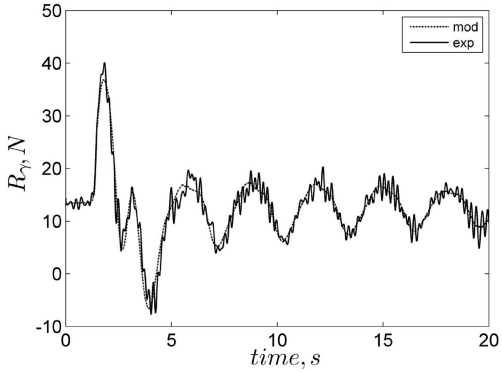

Fig. 10 Comparison between experimental and modeled time histories for R_γ.

routine. On first inspection, results presented for the experimental curve do show a substantial degree of unsteadiness over that obtained from the modeled tangential strut-force time history. From closely considering the data used to construct the experimental time history for R_γ, this unsteadiness was found to originate from having to numerically differentiate the experimental time history of heave angle twice for Eq. (8). With this in mind, however, when comparing the two time histories, the success of the model to accurately predict both the general form of the tangential strut force and its magnitude is clearly evident. A similar result for C_m is shown in Fig. 11.

4. Sensitivity Analysis of Stability Derivatives

To gauge the degree to which the estimated derivatives are influenced by changes in the relevant fundamental parameters detailed in Eqs. (8) and (9), the optimization procedure was again used with selected critical variables changed by $\pm 5\%$ from their mean magnitudes. The variables chosen for this analysis were r, M_{mod}, I_{yy}, V_o, M_{cb}, x, $r_{\text{st}_{\text{c.p.}}}$, $r_{\text{st}_{\text{c.g.}}}$, γ, η, and α, with the base test condition for comparison chosen as $\Delta\eta = 10$ deg. Results from this analysis are presented in Fig. 12.

On first inspection, results for changes in M_{cb}, x, $r_{\text{st}_{\text{c.g.}}}$, and $r_{\text{st}_{\text{c.p.}}}$, are shown to have very little influence on the magnitudes of almost all of the derivatives presented. One possible exception is C_{Lv}; however, the results from this derivative, as already mentioned, were observed to be particularly erratic and/or close to zero magnitude from Fig. 7 and should thus be treated with some caution. Changing freestream velocity by $\pm 5\%$ was curiously found to have a unexpected influence on most of the estimated derivatives, with the magnitudes of the stiffness and control derivatives ranging from $\Delta C_{L\alpha} = 0.183$ to -0.166, $\Delta C_{m\alpha} = -0.0145$ to 0.0126, $\Delta C_{m\eta} = -0.0481$ to 0.0416, and $\Delta C_{L\eta} = 0.0333$ to -0.0366 for $0.95V_o \leq V_o \leq 1.05V_o$, respectively. Expectations were that the nondimensional derivatives would change little with change in freestream velocity; however, this was not evident from the sensitivity analysis conducted and was thought to be due to the nonlinear nature of the PSR/model combination.

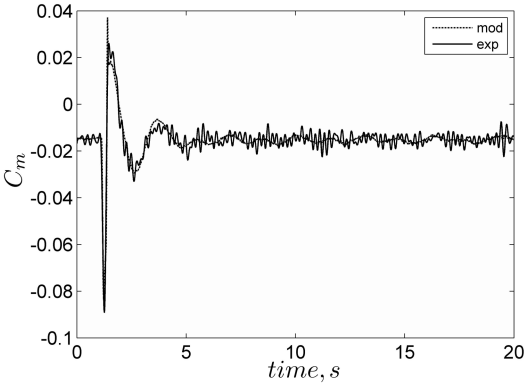

Fig. 11 Comparison between experimental and modeled time histories for C_m.

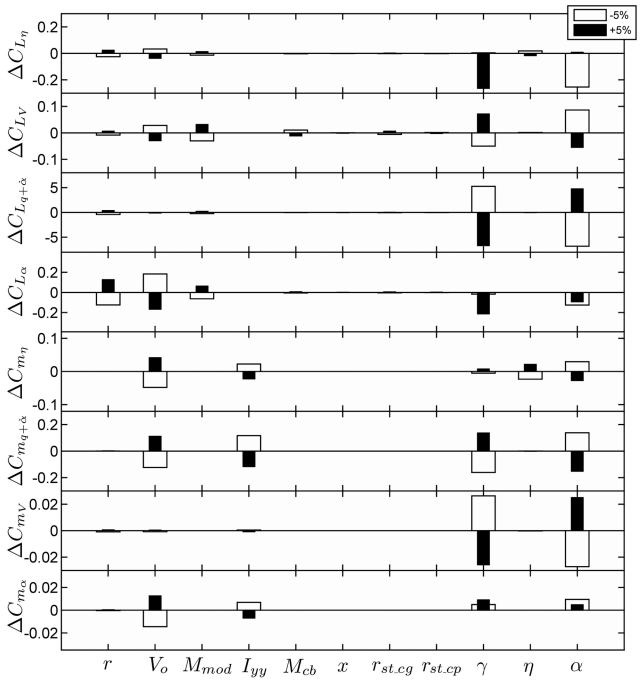

Fig. 12 Sensitivity of stability and control derivatives to selected variable variation of ±5%.

From the remaining results, Fig. 12 shows significant variations in the derivatives presented with change in r, M_{mod} (lift-dependent derivatives only), I_{yy} (pitching-moment-dependent derivatives only), γ, η, and α. As would be expected, all stiffness and control derivatives are influenced through direct changes in α and η, with $\Delta C_{L\alpha} = -0.125$ to -0.0918 and $\Delta C_{m\alpha} = 0.0095$ to 0.0047 for -5 to 5% change in α and $\Delta C_{L\eta} = 0.0186$ to -0.0169 and $\Delta C_{m\eta} = -0.0234$ to 0.0212 for a -5 to 5% change in η. Change in angle of attack is also shown to have a significant influence on both the lift and pitching moment damping derivatives, with maximum changes from the mean reference values presented in Figs. 7 and 8 of -73 to 51% and -5.7 to 6.4% for a change of -5 to 5% in α, respectively. Similar trends in the results presented for a ±5% change in α are also evident for the same corresponding change in PSR angle γ, with the exception that for most of the derivatives presented, a positive change in γ now produces a similar magnitude change but a reversal of direction, compared with the corresponding changes in α.

With regard to the results of Fig. 12, it is clear that the two primary variables affecting the performance of the predicted derivatives using the PSR are γ and α. Although this would be expected, to some degree, as these two variables dictate the forces on the model that drive the model motion (principally from the deflection of η), the assumptions made in Sec. II that the pivot position is coincident with the model c.g. and a.c. need to be considered in the context of the results obtained. Strictly speaking, although these offsets in reality are small, it is envisaged that the moments produced by these offsets in reality will have a some direct influence on the motion of the wind-tunnel test configuration as opposed to conditions that the model would experience in free flight exposed to the same stabilator input deflection. As can be seen from the agreement in the results presented in Figs. 7 and 8, this assumption did not have a large influence on the PSR as a viable technique for the extraction of stability and control derivative, only that, in the author's opinion, these influences must be made as small as possible (taking into account effective initial model stability) to maximize the usefulness and accuracy of the technique.

V. Conclusions

An investigation into the use of a pendulum support rig, which uses an actively controlled model suspended inverted inside a wind tunnel with free movement in model pitch and constrained motion in model heave and forward translation, as a viable tool for the extraction of stability derivative data is presented in this paper. This 2-DOF configuration was shown to perform well at estimating the dominant longitudinal control and stability derivative data when compared against similar tests performed using an established technique and results obtained by the author from a previous investigation. A study conducted into the sensitivity of the system to changes in fundamental input parameters showed that the length of the pendulum strut, freestream velocity, model mass, model moment of inertia, pendulum strut angle, model stabilator angle, and model angle of attack were found to be the most dominant influences on the magnitudes of the estimated derivatives.

Acknowledgments

Funding was provided through the United Kingdom Ministry of Defence under the Applied Research Programme. This work was carried out under the terms of contract CU004-26949 for the Managing Director of Future Systems Technology, QinetiQ, Ltd.

References

[1] Tristant, D., and Beyers, M., "Oscillatory Coning," *Rotary-Balance Testing for Aircraft Dynamics*, AGARD Rept. 265, Neuilly-sur-Seine, France, Dec. 1990.

[2] Jordan, F. L., and Hahne, D. E., "Wind-Tunnel Static and Free-Flight Investigation of High-Angle-of-Attack Stability and Control Characteristics of a Model of the EA-6B Airplane," NASA TP-3194, May 1992.

[3] Young, J., and Lai, J. C. S., "Oscillation Frequency and Amplitude Effects on the Wake of a Plunging Airfoil," *AIAA Journal*, Vol. 42, No. 10, 2004, pp. 2042–2052. doi:10.2514/1.5070

[4] Ahn, S., Choi, K.-Y., and Simpson, R., "Design and Development of a Dynamic Pitch-Plunge Model Mount," 27th Aerospace Sciences Meeting, Reno, NV, AIAA Paper 89-0048, Jan. 1989.

[5] Owens, D. B., Capone, F. J., Hall, R. M., Brandon, J. M., and Chambers, J. R., "Transonic Free-to-Roll Analysis of Abrupt Wing Stall on Military Aircraft," *Journal of Aircraft*, Vol. 41, No. 3, 2004, pp. 474–484. doi:10.2514/1.3073

[6] Capone, F. J., Owens, D. B., and Hall, R. M., "Development of a Transonic Free-to-Roll Test Capability," *Journal of Aircraft*, Vol. 41, No. 3, 2004, pp. 456–463. doi:10.2514/1.1449

[7] Rajamurthy, M., "Generation of Comprehensive Longitudinal Aerodynamic Data Using Dynamic Wind-Tunnel Simulation," *Journal of Aircraft*, Vol. 34, No. 1, 1997, pp. 29–33. doi:10.2514/2.2157

[8] Balakrishna, S., Niranjana, T., Rajamurthy, M. S., Srinathkumar, S., Rajan, S. R., and Singh, S. K., "Estimation of Aerodynamic Derivatives Using Dynamic Wind Tunnel Simulation Technique," *Deutschen Zentrums für Luft- und Raumfahrt*, Rept. 93-14, Brunswick, Germany, Dec. 1993, pp. 289–298.

[9] Gili, P. A., and Battipede, M., "Experimental Validation of the Wing Dihedral Effect Using a Whirling Arm Equipment," *Journal of Aircraft*, Vol. 38, No. 6, 2001, pp. 1069–1075. doi:10.2514/2.2874

[10] Taylor, G. S., Gursul, I., and Greenwell, D. I., "Investigation of Support Interference in High-Angle-of-Attack Testing," *Journal of Aircraft*, Vol. 40, No. 1, 2003, pp. 143–152. doi:10.2514/2.3069

[11] Van Dam, C. P., Fremaux, C. M., and Dalbello, T., "Simulation of Flow About Rotating Forebodies at High Angles of Attack," *Journal of Aircraft*, Vol. 41, No. 6, 2004, pp. 1298–1305. doi:10.2514/1.8984

[12] Hahne, D. E., Wendel, T. R., and Boland, J. R., "Wind-Tunnel Free-Flight Investigation of a Supersonic Persistence Fighter," NASA TP-3258, Feb. 1993.

[13] Bennett, R., Farmer, M., Mohr, R., and Hall, W., "Wind-Tunnel Technique for Determining Stability Derivatives from Cable-Mounted Models," *Journal of Aircraft*, Vol. 15, No. 5, 1978, pp. 304–310. doi:10.2514/3.58360

[14] Magill, J. C., Cataldi, P., Morency, J. R., Hammer, D. X., and Anderson, B. D., "Design of a Wire Suspension System for Dynamic Testing in AEDC 16T," 41st Aerospace Sciences Meeting and Exhibit, Reno, NV, AIAA Paper 2003-0452, Jan. 6–9, 2003.

[15] Cook, M. V., "On the Use of Small Scale Aircraft Models for Dynamic Wind Tunnel Investigation of Stability and Control," *Transactions of*

the Institute of Measurement and Control (London), Vol. 9, No. 4, 1987, pp. 190–197.
doi:10.1177/014233128700900405

[16] Subke, H., "Test Installations to Investigate the Dynamic Behavior of Aircraft with Scaled Models in Wind Tunnels," *Transactions of the Institute of Measurement and Control (London)*, Vol. 1, No. 3, 1979, pp. 135–140.
doi:10.1177/014233127900100302

[17] Magill, J., Darden, L., and Komerath, N., "Flow Visualization During Multiple-Axis Motions Using a Wind-Driven Manipulator," *Journal of Aircraft*, Vol. 33, No. 1, 1996, pp. 163–170.
doi:10.2514/3.46917

[18] Pedreiro, D., "Development of an Apparatus for Wind Tunnel Dynamic Experiments at High Alpha," NASA CR-203713, Feb. 1997.

[19] Goman, M., Kolinko, K., Khrabrov, A., and Usoltsev, S., "Investigation of Dynamics and Unsteady Aerodynamic Characteristics of Movable Aircraft Model on Pendulum Support in a Wind Tunnel," *International Conference on Fundamental Research in Aerospace Science*, TsAGI, Moscow, 1992.

[20] Goman, M., "Mathematical Modeling of High Angles of Attack Aerodynamics for Solving Flight Dynamics Problems," De Montford Univ., School of Computing Sciences, Research Monograph 13, Leicester, England, U.K., 1997.

[21] Davidson, P., Lowenberg, M. H., and di Bernardo, M., "Experimental Analysis and Modeling of Limit Cycles in a Dynamic Wind Tunnel Rig," *Journal of Aircraft*, Vol. 40, No. 4, 2003, pp. 776–785.
doi:10.2514/2.3158

[22] Kyle, H., "An Investigation into the Use of a Pendulum Support Rig for Aerodynamic Modeling," Ph.D. Dissertation, Dept. of Aerospace Engineering, Univ. of Bristol, Bristol, England, U.K., 2004.

[23] Lowenberg, M., and Kyle, H., "Development of a Pendulum Support Rig Dynamic Wind Tunnel Apparatus," AIAA Atmospheric Flight Mechanics Conference and Exhibit, AIAA Paper 2002-4879, Monterey, CA, 5–8 Aug. 2002.

[24] Gatto, A., and Lowenberg, M. H., "Evaluation of a Three Degree of Freedom Test Rig for Stability Derivative Estimation," *Journal of Aircraft*, Vol. 43, No. 6, 2006, pp. 1747–1761.
doi:10.2514/1.19821

[25] Cook, N. J., "A Sensitive 6-Component High-Frequency-Range Balance for Building Aerodynamics," *Journal of Physics E: Scientific Instruments*, Vol. 16, No. 5, 1983, pp. 390–393.
doi:10.1088/0022-3735/16/5/007

[26] Optimization Toolbox, Software Package, Ver. 4, The MathWorks, Inc., Natick, MA, 2008.

[27] Coleman, T. F., and Li, Y., "An Interior, Trust Region Approach for Nonlinear Minimization Subject to Bounds," *SIAM Journal on Optimization*, Vol. 6, No. 2, 1996, pp. 418–445.
doi:10.1137/0806023

[28] Coleman, T. F., and Li, Y., "On the Convergence of Reflective Newton Methods for Large-Scale Nonlinear Minimization Subject to Bounds," *Mathematical Programming*, Vol. 67, Nos. 1–3, 1994, pp. 189–224.
doi:10.1007/BF01582221

[29] O'Leary, C. O., "Wind-Tunnel Measurement of Aerodynamic Derivatives Using Flexible-Sting Rigs," *Dynamic Stability Parameters*, AGARD Rept. LS 114, Neuilly-sur-Seine, France, Mar. 1981.

[30] O'Leary, C. O., "Oscillatory Data for Typical Configurations," *Special Course on Aircraft Dynamics at High Angles of Attack: Experiments and Modelling*, AGARD Rept. 776, Neuilly-sur-Seine, France, Apr. 1991.

[31] O'Leary, C. O., "Relation Between Rotary and Oscillatory Test Results," *Rotary-Balance Testing for Aircraft Dynamics*, AGARD Rept. 265, Neuilly-sur-Seine, France, Dec. 1990.

[32] Klien, V., and Morelli, E. A., *Aircraft System Identification, Theory and Practice*, AIAA Education Series, AIAA, Reston, VA, 2006, Chap. 3, pp. 27–73.

[33] Schmidt, L. V., *Introduction to Aircraft Flight Dynamics*, AIAA Education Series, AIAA, Reston, VA, 1998, pp. 15–67.